Title

Cell contractility drives mechanical memory of oral squamous cell carcinoma

Journal

Molecular Biology of the Cell, 34(9)

ISSN

1059-1524

Authors

Moon, So Youn

de Campos, Paloma Santos

Matte, Bibiana Franzen

et al.

Publication Date

2023-08-01

DOI

10.1091/mbc.e22-07-0266

Peer reviewed

Cell contractility drives mechanical memory of oral squamous cell carcinoma

So Youn Moon[a,b,†], Paloma Santos de Campos[c,†], Bibiana Franzen Matte[c], Jesse K. Placone[a,d], Virgílio G. Zanella[c,e], Manoela D. Martins[c], Marcelo Lazzaron Lamers[c,f,*], and Adam J. Engler[a,b,*]
[a]Department of Bioengineering, University of California San Diego, La Jolla, CA 92093; [b]Sanford Consortium for Regenerative Medicine, La Jolla, CA 92037; [c]Department of Oral Pathology, Federal University of Rio Grande do Sul, [e]Department of Head and Neck Surgery, Santa Rita Hospital, Santa Casa de Misericórdia de Porto, Alegre, and [f]Deparment of Morphological Sciences, Institute of Basic Health Sciences, Federal University of Rio Grande do Sul, Porto Alegre, RS 90035, Brazil; [d]Department of Physics and Engineering, West Chester University of Pennsylvania, West Chester, PA 19383

ABSTRACT **Matrix stiffening is ubiquitous in solid tumors and can direct epithelial–mesenchymal transition (EMT) and cancer cell migration. Stiffened niche can even cause poorly invasive oral squamous cell carcinoma (OSCC) cell lines to acquire a less adherent, more migratory phenotype, but mechanisms and durability of this acquired "mechanical memory" are unclear. Here, we observed that contractility and its downstream signals could underlie memory acquisition; invasive SSC25 cells overexpress myosin II (vs. noninvasive Cal27 cells) consistent with OSCC. However, prolonged exposure of Cal27 cells to a stiff niche or contractile agonists up-regulated myosin and EMT markers and enabled them to migrate as fast as SCC25 cells, which persisted even when the niche softened and indicated "memory" of their prior niche. Stiffness-mediated mesenchymal phenotype acquisition required AKT signaling and was also observed in patient samples, whereas phenotype recall on soft substrates required focal adhesion kinase (FAK) activity. Phenotype durability was further observed in transcriptomic differences between preconditioned Cal27 cells cultured without or with FAK or AKT antagonists, and such transcriptional differences corresponded to discrepant patient outcomes. These data suggest that mechanical memory, mediated by contractility via distinct kinase signaling, may be necessary for OSCC to disseminate.**

Monitoring Editor
Michael Murrell
Yale University

Received: Jul 11, 2022
Revised: Jun 6, 2023
Accepted: Jun 15, 2023

INTRODUCTION

There are more than 350,000 new oral and pharynx cancer cases and 177,000 deaths annually worldwide (Bray *et al.*, 2018), and oral squamous cell carcinoma (OSCC) represents 80–90% of all malignant tumors of the oral cavity (Johnson *et al.*, 2011; Pires *et al.*, 2013; Jensen *et al.*, 2019), with a 5-y survival rate that varies from 40 to 63% (Kamangar *et al.*, 2006; Scully and Bagan, 2009; Warnakulasuriya, 2009; Montero and Patel, 2015). Oral lesions are clinically characterized by dysplastic regions with irregular rigid margins

This article was published online ahead of print in MBoC in Press (http://www.molbiolcell.org/cgi/doi/10.1091/mbc.E22-07-0266) on June 21, 2023.

Conflict of interest: The authors declare that there is no conflict of interests.

[†]These authors contributed equally to this work.

Author contributions: P.S.C., S.Y.M., M.L.L., and A.J.E. conceived of various aspects of the project. P.S.C., S.Y.M., B.F.M., and J.K.P. performed all experiments. Patient samples were provided by V.G.Z. and M.D.M. and analyzed by P.S.C. S.Y.M. performed all TCGA analyses. Experiments were designed and the manuscript was written by P.S.C., S.Y.M., M.L.L., and A.J.E. with input from the other authors.

*Address correspondence to: Marcelo Lazzaron Lamers (marcelo.lamers@ufrgs.br); Adam J. Engler (aengler@ucsd.edu).

Abbreviations used: AKT, protein kinase B; BCA assay, bicinchoninic acid assay used for protein quantification; CT, center of the tumor; DEG, differentially expressed gene; ECM, extracellular matrix; EDTA, ethylenediaminetetraacetic acid; EMT, epithelial-mesenchymal transition; FAK, focal adhesion kinase; FBS, fetal bovine serum; GO, gene ontology; IF, Immunofluorescence; IZ, invasive boarder zone; LPA, lysophosphatidic acid; MLCK, myosin light chain kinase; NMM, nonmuscle myosin; OSCC, oral squamous cell carcinoma; PA, polyacrylamide; PAAGS, polyacrylamide gel substrate; PBS, phosphate-buffered saline; PCR, polymerase chain reaction; RIN number, RNA integrity number; RNA, ribonucleic acid; SCC, squamous cell carcinoma; SHG imaging, second-harmonic generation imaging; TAE, tumor adjacent epithelium; TC, tumor core; TCGA, the cancer genome atlas; TNM, a system to describe the amount and spread of cancer in a patient's body; T, the size of the tumor and any spread of cancer into nearby tissue; N, spread of cancer to nearby lymph nodes; M, metastasis; UV, ultraviolet.

(Chi *et al.*, 2015). Extracellular matrix (ECM) up-regulation and cross-linking–relative to softer tumor–adjacent epithelium (TAE)–create the stiff tumor border, which has been observed in a variety of other tumors including OSCC (Frantz *et al.*, 2010; Boudreau *et al.*, 2012; Lu *et al.*, 2012; Bonnans *et al.*, 2014; Yu *et al.*, 2019). ECM up-regulation is correlated with poor patient outcomes (Wei *et al.*, 2015; Burgstaller *et al.*, 2017; Matte *et al.*, 2019) and increased invasive potential (Paszek *et al.*, 2005; Chaudhuri *et al.*, 2014; Wei *et al.*, 2015; Ondeck *et al.*, 2019), but to date in the context of OSCC, this link and the mechanisms that regulate it have not been clearly articulated.

For cancer cells to sense and respond to ECM stiffness, communication between extracellular and intracellular compartments is necessary (Hanahan and Weinberg, 2011; Pickup *et al.*, 2014). These compartments are mechanically linked by transmembrane integrins that connect the ECM with actin cytoskeleton and ultimately the nucleus via adhesion, contractile and signaling proteins (Parsons *et al.*, 2010). Although stiffness sensing mechanisms are well established in other cancers, for example, kinases in breast (Levental *et al.*, 2009; Calvo *et al.*, 2013; Fattet *et al.*, 2020), brain (Umesh *et al.*, 2014; Wong *et al.*, 2015; Liu *et al.*, 2018), and ovarian (Wei *et al.*, 2021) cancers among others, relatively little is known about OSCC. Typically, these outside-in mechanisms establish a positive feedback loop whereby nonmuscle myosin-II (NMM2) contractility modulates adhesions and integrin/ECM binding to further enhance signaling, contraction, and migration (Vicente-Manzanares *et al.*, 2008; Wu *et al.*, 2009). Stiffness-mediated signaling can result in cytoskeletal assembly changes and force transduction to the nucleus, which impacts gene transcription and epithelial–mesenchymal transition (EMT) (Wang *et al.*, 2009; Chin *et al.*, 2016; Stowers *et al.*, 2019). For example, stiffer substrates can induce tumorigenesis in mammary epithelial cells via altered chromatin accessibility resulting from hypercontractile cells (Stowers *et al.*, 2019). In lung tumors, stiffness enhances expression of EMT genes (Tilghman *et al.*, 2010; Alonso-Nocelo *et al.*, 2018). These dynamic interactions can even enhance tumor growth, survival, and invasion (Geiger *et al.*, 2001; Paszek *et al.*, 2005; Butcher *et al.*, 2009).

Once outside of their stiffened niche, however, cancer cells must also be able to maintain their stiffness-induced EMT, that is, invading mesenchymal-like cells retain marker expression and migratory potential. This ability to form "mechanical memories" has been shown in mammary epithelial cells, which after preconditioning on a stiff matrix, migrate faster, up-regulate contractile proteins, and maintain EMT on a soft matrix (Nasrollahi *et al.*, 2017). In dynamic contexts though, signaling becomes more complicated; in multicellular mammary spheroids or in matrix that stiffens with time, multiple redundant signaling pathways may collectively regulate EMT in mammary epithelial cells (Ondeck *et al.*, 2019). We previously showed that poorly invasive OSCC cell lines can acquire a more migratory phenotype in a stiffer environment (Matte *et al.*, 2019), that is, 20 kilopascal (kPa), which mirrors the stiffest regions of dysplastic oral tumors (Zhang *et al.*, 2020). How such oral cells develop stiffness-mediated responses and whether they retain "memory" of their tumor-like niche when on softer matrix, that is, 0.5 kPa, has not been thoroughly explored in OSCC. Herein, we demonstrate that a noninvasive oral epithelial cell line, that is, Cal27, can undergo EMT and acquire "memory" from stiff matrix that enables cells to maintain their new phenotype despite being on a softer niche. Protein kinase B (AKT) and focal adhesion kinase (FAK) play key roles in this process, which could be maintained for days in culture and are reflected in transcriptomic differences that corresponded to patient outcomes.

RESULTS

Contractility regulates the acquisition of mechanical memory

Increased cell contractility typically occurs as a result of EMT (Parsons *et al.*, 2010; Friedl *et al.*, 2012; Aguilar-Cuenca *et al.*, 2014; Newell-Litwa *et al.*, 2015), but it is unclear in OSCC. To establish to what extent and where contractile machinery is present in OSCC and their derivative cell lines, we analyzed nonmuscle myosin isoform expression in OSCC biopsies. NMM2B was detected at the basal cell layer and staining was strongest in cells at the invasive front of the tumor (Figure 1A; Supplemental Table S1). Both patients–being of advanced stage IV–corroborate prior findings that tumors of more advanced tumor-node-metastasis (TNM) stages express higher NMM2B (Dias *et al.*, 2019). In oral cell lines, NMM2A and B were expressed more in mesenchymal SCC25 versus epithelial Cal27 cells (Figure 1B). To study how contractile machinery plays role in Cal27 acquiring mesenchymal-like phenotypes from stiff environment (Matte *et al.*, 2019), lysophosphatidic acid (LPA), which stimulates contraction through its receptor's downstream signaling via Rho/RCK, and Blebbistatin, a nonmuscle myosin inhibitor, were used along with exposure to substrates with varying stiffness. Culture of epithelial Cal27 cells on stiffer matrix or with LPA had similar effects on morphology and phenotype, leading to more compact cell colonies and higher EMT marker expression, versus culture on soft matrix or with Blebbistatin (Figure 1, C and D). These results together suggest that the acquisition of more mesenchymal-like behavior, concurrent with our prior observations (Matte *et al.*, 2019), may be the result of higher myosin and EMT marker expression.

Invasion requires that cells leave the tumor niche. Hence, they must have durable expression of stiffness-mediated EMT markers once in the TAE, that is, "mechanical memory"; while present in other carcinomas (Nasrollahi *et al.*, 2017), we sought to test this in OSCC cell lines and assess the impact contractility has on memory. Cal27 cells were conditioned on soft or stiff substrates for 5 d and replated onto soft substrate for an additional day (Figure 2A). Relative to mesenchymal SCC25 cells, we found that E-cadherin peripheral localization was highest in Cal27 cells on soft matrix, which is an indicator of an epithelial phenotype, and was markedly reduced for cells preconditioned on stiff matrix. Conversely, those cells preconditioned on stiff substrates had statistically higher NMM2A expression than their soft substrate counterparts and were not different from mesenchymal SCC25 cells (Figure 2B–D). This reciprocal relationship suggests that stiff preconditioning could enable cells to acquire and maintain their prior mesenchymal phenotype despite TAE-like stiffness. This interpretation may also be consistent with cell migration after replating (Figure 3A); Cal27 cells preconditioned on a stiff niche or first treated with LPA retained higher migration velocity and explored a larger substrate area, whether migrating collectively or individually in 2D. Conversely, when Cal27 cells were cultured with a contractile antagonist such as Blebbistatin after replating from a stiff to a soft hydrogel, cells typically responded by failing to maintain higher migration velocities (Figure 3, B and C). These data, at least in 2D, suggest contractile regulation of mechanical sensing and maintenance of a stiffness-induced mesenchymal phenotype. Further consistent with this interpretation in 3D, preconditioned Cal27 cells were induced to form spheroids and then embedded into a collagen matrix. Those spheroids from cells plated originally on stiff hydrogels or that were treated with LPA were more invasive over five subsequent days of culture than their counterparts on soft matrix only or when cultured with Blebbistatin (Figure 3, D and E).

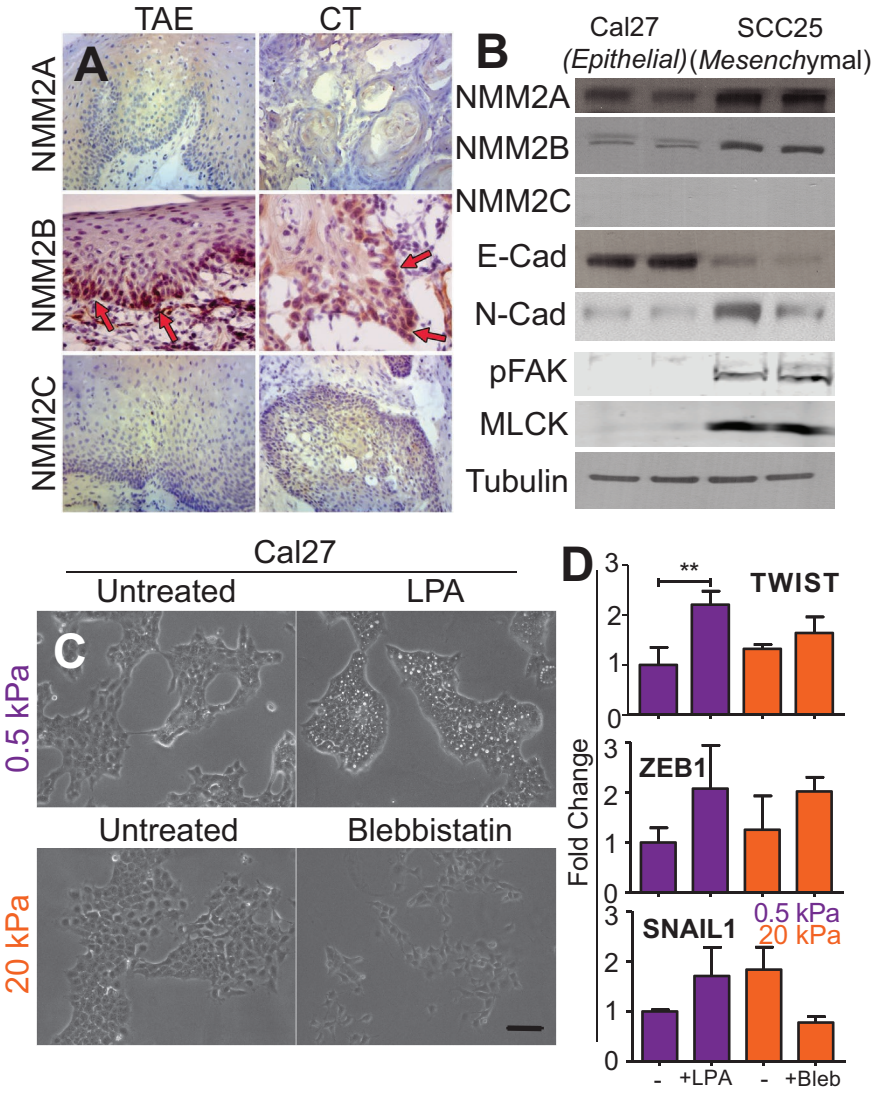

FIGURE 1: Contractility modifies cell behavior in oral squamous carcinoma in vivo and increases EMT marker expression in vitro. (A) Immunohistochemistry staining for nonmuscle myosin (NMM) IIA, IIB, and IIC in TAE and CT. Red arrows indicate positive staining (brown) ($n = 15$). (B) Representative Western blots for NMM 2A, 2B, and 2C, as well as E-cadherin, N-cadherin, pFAK, MLCK, and tubulin in low (Cal27; epithelial) or high (SCC25; mesenchymal) invasive OSCC cell lines. (C) Brightfield images of Cal27 cells after 5 d of culture on soft (0.5 kPa) or stiff substrates. Cells were selectively treated with Blebbistatin (10 μM) and LPA (10 μM) as indicated. Scale bar is 100 μm. (D) Fold change to mRNA expression is plotted for the indicated transcription factors, substrate stiffness (purple = 0.5 kPa; orange = 20 kPa), and drug treatment. All data are shown from triplicate biological replicates and were normalized to GAPDH and then to the soft control (0.5 kPa; far left). $^{**}P < 0.01$ via one-way analysis of variance with Tukey's posttest. CT, center of the tumor; LPA, lysophosphatidic acid; TAE, tumor-adjacent epithelium.

Taken together, 2D and 3D assays suggest that high cell contractility in soft environments may artificially induce mesenchymal-like responses that imply a sort of "mechanical memory" whereas contractile inhibition during preconditioning may block acquisition of such memory.

Acquisition and recovery of mechanical memory, respectively, involve AKT and FAK signaling

To identify signaling pathway(s) involved in stiffness-mediated phenotype changes, we analyzed 43 phospho-proteins and found activity at 11 sites, that is, signal greater than twofold above background, of which AKT (S308)—a pathway involved in OSCC migration (Fujii *et al.*, 2020)—was the most phosphorylated when Cal27 cells that were maintained on soft matrix were replated onto stiff matrix for an hour. Conversely, Cal27 cells that were maintained on stiff matrix and then replated onto soft matrix for an hour had 23 sites above background; of those, FAK (Y397), which is required for OSCC stiffness sensing (Zhang *et al.*, 2021), was one of the most phosphorylated site when memories of the stiff substrate were "recalled" (Figure 4A). Contractility and signaling differences could cause larger transcriptomic differences between preconditioned Cal27 cells ("Learn") and those exposed to inhibitors ("Don't Learn/Forget"). RNA sequencing of these two groups revealed 822 differentially expressed genes (DEGs; $-0.1 > FC > 0.1$, p-val < 0.1) between "Learn" and "Don't Learn/Forget" groups (Figure 4B; Supplemental Table S1). We mapped Gene Ontology (GO) terms onto these DEGs and found that the top 20 terms primarily associated with cellular components of the cytoskeleton and ECM and with biological processes associated with migration (Figure 4C; Supplemental Table S2). A total of 112 genes within the top GO terms were significantly and/or differentially expressed as highlighted by an MA plot (Supplemental Figure S2A, purple/green data; Supplemental Table S3). For six of the most significantly and/or differentially expressed genes (above/below or to the right of dashed lines in panel B; i.e., *SDC4*, *ICAM1*, *FN1*, and *ITGAV* for up-regulated and *RhoD* and *FSCN1* to be down-regulated in "Learn" group), we further validated expression via qPCR, finding linear correlation between sequencing and qPCR (Supplemental Figure S2B). Those significantly and/or differentially expressed genes (Supplemental Table S4), which may form a minimal grouping of genes related to mechanical memory, were then used to stratify patients in The Cancer Genome Atlas (TCGA). To ensure a robust patient population, the expression profiles for all head–neck squamous carcinomas, including OSCC, were computed ($n = 155$), and between the top and bottom expression quintiles, progression-free interval (Figure 4D) and overall survival (Figure 4E) showed significant differences. These data suggest that there is perhaps a common transcriptomic signature that results from contractility-based preconditioning, which could be used to screen patient tumors for signs of "memory" in addition to conventional histology.

Based on GO terms mapped on DEGs in which cell adhesion junction and cell migration/motility are different between "Learn" and "Don't Learn/Forget" (Supplemental Table S2), cell adhesion and migration difference of Cal27 were assessed to study how AKT or FAK pathways are related to those cell functions and further affect mechanical memory acquisition processes. Although adhesion strength was not significantly different (Supplemental

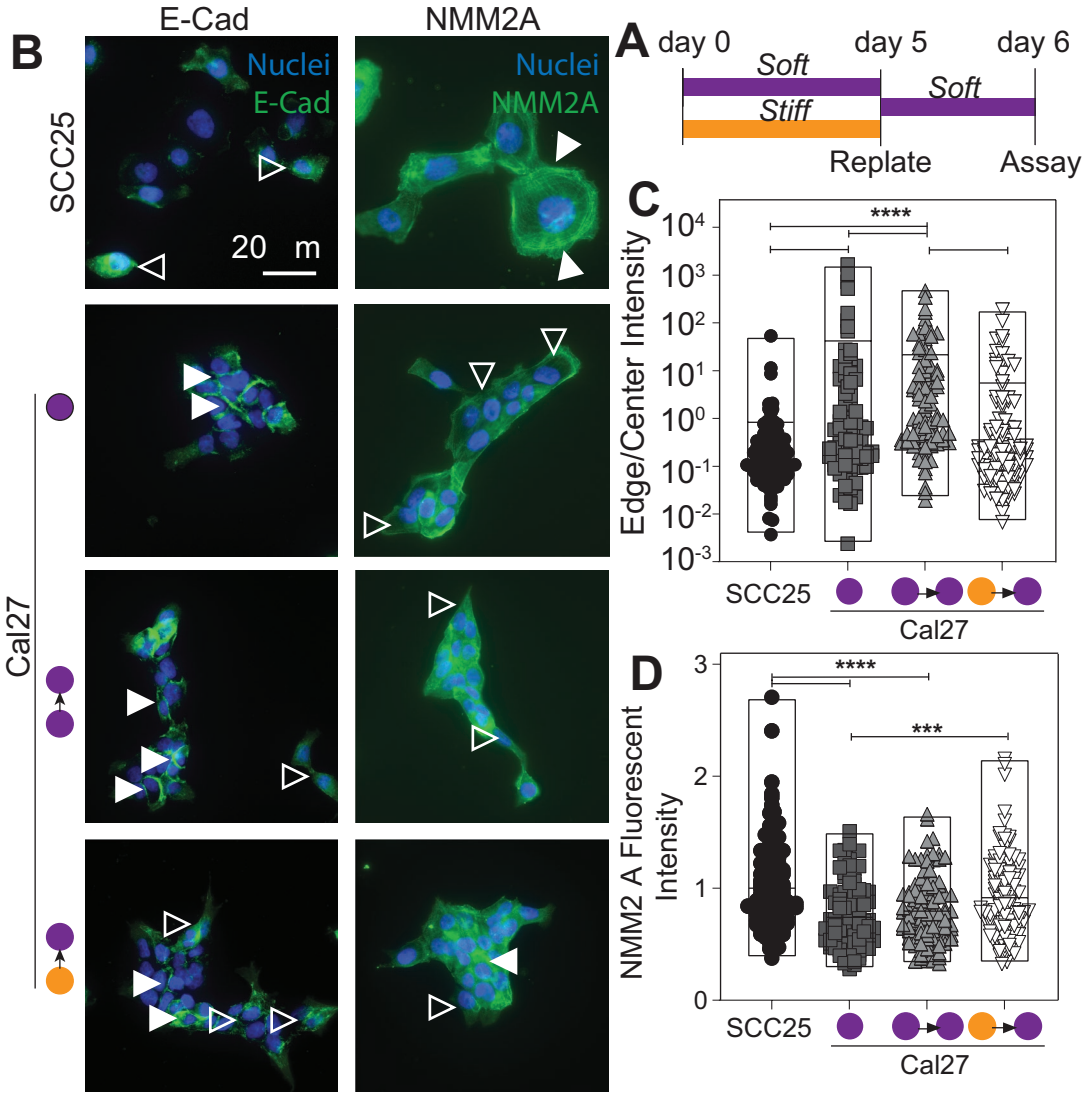

FIGURE 2: Stiffness-induced changes in E-cadherin localization and NMM2 expression are durable in tissue-adjacent epithelium–like stiffness. (A) Experimental design of cell preconditioning and replating on stiff (orange) or soft (purple) substrates. (B) Immunofluorescence images are shown of SCC 25 cells (top) and Cal27 cells on soft substrate (top middle), without preconditioning (bottom middle), and with stiff preconditioning (bottom). Cells were stained in green for E-cadherin (left column) and NMM2A (right column) and blue for nuclei (DAPI). Scale bar is 20 μm. Open arrowheads indicate cells with less peripheral E-cadherin or lower myosin expression whereas filled arrowheads indicate cells with more peripheral E-cadherin or higher myosin expression. (C) Plot of edge to center pixel intensity ratio for the conditions from panel B. Box plot shows mix, max, and mean values along with individual data points ($n = 124$, 112, 96, and 117, left to right, respectively). (D) Plot of NMM2A fluorescent intensity for the conditions from panel B. Data are normalized to average intensity of SCC25 for each biological replicate. Box plot shows mix, max, and mean values along with individual data points ($n = 136$, 126, 117, and 131, left to right, respectively). ***$p < 10^{-2}$; ****$p < 10^{-3}$ via one-way analysis of variance with Tukey's posttest.

Figure S3), we found a titratable influence on migration; specifically, inhibition of AKT (≥5-μM AKT inhibitor) significantly reduced both collective and individual migration speed of cells conditioned on soft and then replated to stiff matrix (Supplemental Figure S4A), and inhibition of FAK (≥10-μM FAK inhibitor) pathway discouraged cell migration after being replated from stiff to soft matrix (Supplemental Figure S4B). When combined with stiff substrates or cultured with LPA, AKTi-treated Cal27 cells failed to "learn" or exhibit higher migration speed when replated (Figure 5A) similar to blocking contractility with Blebbistatin (Figure 5B). Conversely, replated Cal27 cells that were then treated with FAKi also failed to exhibit higher migration speed (Figure 5, A and B) or could not recall the impact of prior mesenchymal transitions and "forgot." Thus, both groups—one with impaired contractility and the other with an inhibited signaling pathway that up-regulated during memory recovery—had significantly slower cell migration speed than the group conditioned on stiff substrates.

Validation of this mechanism in human tumors is critical to establishing its importance; hence, 19 OSCC tumors were assessed in their core and invasive zones for AKT phosphorylation (Figure 5C) and collagen organization (as a surrogate for tumor rigidity [Wei *et al.*, 2015]). Tumor cores were generally positive for AKT phosphorylation at S308, independent of TNM tumor stage. However, when stratifying by stage and collagen organization, only stage III/IV

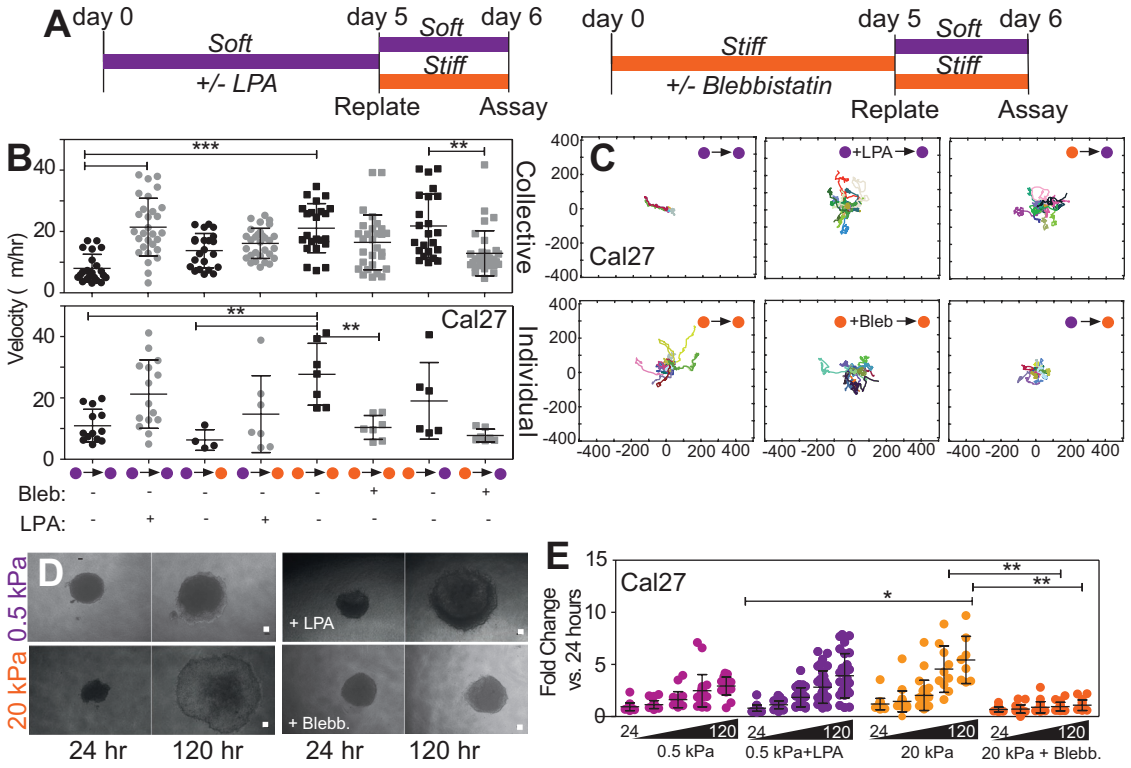

FIGURE 3: Acquisition of mechanical memory in 2D and 3D environment is affected by contractility. (A) Experimental design of cell preconditioning and replating on stiff (orange) or soft (purple) substrates. (B) Collective (top) and individual (bottom) migration velocity was analyzed for Cal27 cells on stiffness combinations (soft = purple; stiff = orange) and/or treatment with LPA (10 μM) or Blebbistatin (10 μM) as indicated (n = 22, 29, 22, 30, 23, 29, 23, and 32 cells for collective migration, and n = 13, 15, 4, 7, 7, 7, 6, and 7 cells for individual migration, left to right). (C) Rose plots of collective cell migration on stiffness combinations (soft = purple; stiff = orange) and/or treatment with LPA (10 μM) or Blebbistatin (10 μM) as indicated. Each line represents one cell trajectory. Axes indicate distance in μm. Fold change to OSCC spheroids preconditioning in soft and stiff substrate (control and treated with LPA/Blebbistatin) normalized to 24-h sphere. (D) Brightfield images at 24 and 120 h of culture and (E) plots of OSCC-derived spheroid migration on soft (purple) or stiff (orange) substrates and treatment with LPA (10 μM) or Blebbistatin (10 μM) as indicated. Scale bar is 50 μm. *$p < 0.05$; **$p < 0.01$; ***$p < 0.001$ for all data as analyzed by one-way analysis of variance with Tukey's posttest. LPA, lysophosphatidic acid.

tumors had statistically higher percentages of cells phosphorylating S308 on AKT in the core versus adjacent invasive zone. For lower staged tumors or those with disorganized collagen, even cells in the adjacent invasive zone had phosphorylated AKT(S308) (Figure 5D). The lack of phosphorylation differences suggests that tumors may be soft enough and that cells do not develop sufficient "memory" in the core, which could corroborate the involvement of AKT pathway in the memory-learning process for stiff, high-grade tumors.

DISCUSSION

Bidirectional cross talk between tumor cell and ECM can change cell behavior; thus, ECM dynamics can modify cell phenotypes and promote malignancy (Van Helvert *et al.*, 2018; Yamada and Sixt, 2019). Increased tissue stiffness is a well-known feature of tumors (Lu *et al.*, 2012), and its potential to drive malignant transition in tumor cells has been studied in several tumor sites (Butcher *et al.*, 2009; Baker *et al.*, 2013; Chen *et al.*, 2015). However, interaction between ECM stiffness and OSCC has not been deeply explored yet, so here we studied how OSCC cells are affected by matrix stiffness as its changes when transitioning from stiffer tumor to softer TAE. We had previously found that noninvasive Cal27 oral epithelial cells demonstrate increased cell migration velocity by being conditioned on stiff matrix (Matte *et al.*, 2019), and here, we extended that work to observe that Cal27 cells preconditioned on stiff matrix not only adopt a more mesenchymal-like phenotype but also then maintain that expression for days more on softer substrates due to their prolonged ability to regulate contractility via AKT and FAK pathways. Not only did we then observe correlations with collagen organization differential AKT phosphorylation between tumor core and TAE, and tumor staging, but also found that the stiff niche promoted a durable transcriptional change that correlated with patient outcomes.

Although our data suggest that oral epithelial cell phenotype can be regulated by contractility, it is by no means a novel or exclusive mechanism. Contractile forces regulate a variety of processes ranging from embryogenesis to pathogenesis and are the result of cells modulating myosin activity (Butcher *et al.*, 2009; Wozniak and Chen, 2009; Parsons *et al.*, 2010). Within a cancer context, tumor progression has been shown to correlate with NMM2 expression, enabling cell migration and accelerating turnover of cell–cell adhesion (Peglion *et al.*, 2014). We previously found a similar inverse relationship between adhesion and contraction when Cal27 cells were conditioned by stiffness for 5 d (Matte *et al.*, 2019) as well as in breast cancer cells sorted by adhesion. There, less adhesive cells

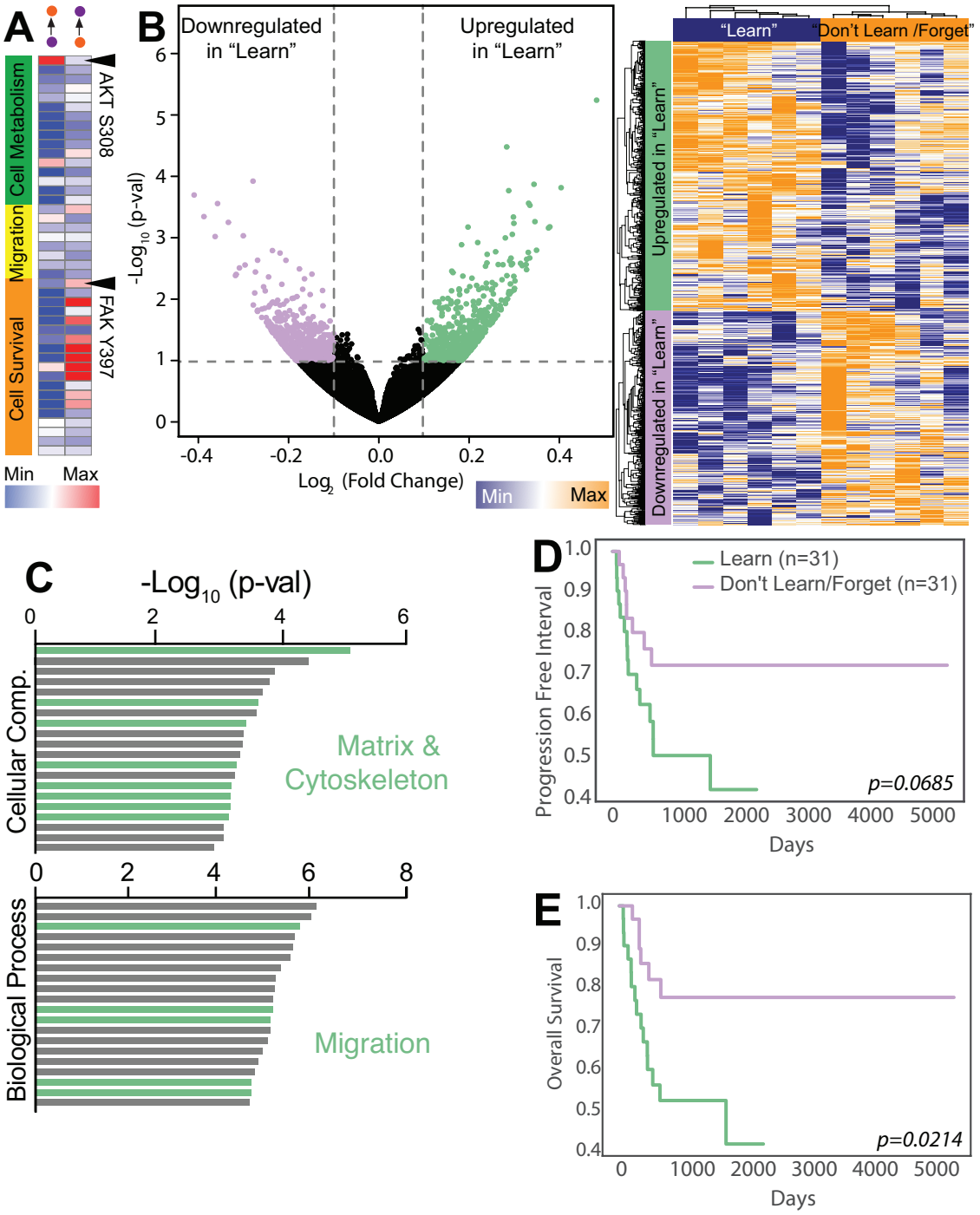

FIGURE 4: Phospho-protein array and transcriptomic differences suggest that mechanical memory involves AKT and FAK signaling. (A) Heat map of spot intensity from an array of 43 phosphorylation sites. Cal27 cell lysates were blotted, and cells had been switched from soft to stiff ("learn"; left) or stiff to soft substrate ("recall"; right) for 1 h. Data are normalized to Cal27 cells cultured on their original substrate, that is, soft and stiff, respectively. Red indicates up-regulation and blue indicates down-regulation relative to lysate from the original substrate. (B) Volcano plot (left) and heat map (right) of the genes from bulk RNA sequencing. In volcano plot, up(green)-/down(purple)-regulated genes in "Learn" groups were identified and marked with $\log_2$ fold change of >0.1 and $-\log_{10}$ *p* value of >1. Heat map of shows the hierarchical clustering of differentially expressed genes identified from the volcano plot. (C) Gene ontological terms determined from DEGs in panel A. Terms shown in green indicate those associated with matrix and cytoskeleton (cellular component) and adhesion and migration (biological processes). (D, E) Data above/below (i.e., ($\log_2$ [fold change] > 0.3) and/or to the right (i.e., $\log_2$ [expression] > 13) of dashed lines in Supplemental Figure S2A were identified as highly expressed or highly differentially expressed, were further validated in Supplemental Figure S2B, and used here to stratify patients in The Cancer Genome Atlas (TCGA). Plots show progression-free interval and overall survival as indicated. Significance show in plots is based on a log-rank (Mantel–Cox) test.

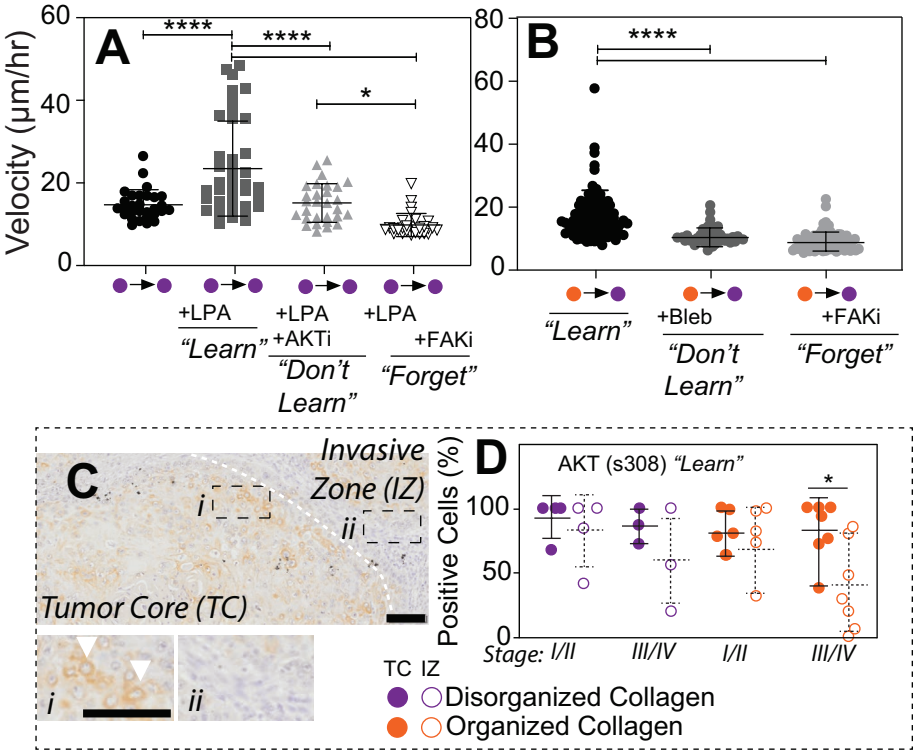

FIGURE 5: Functional and phenotypic differences between "Learn" and "Don't Learn/Forget" groups. (A, B) Collective migration velocity was plotted for Cal27 cells on stiffness combinations as indicated (soft = purple; stiff = orange) plus selective treatment with AKT or FAK inhibitors, with contractile agonist LPA, or with contractile antagonist Blebbistatin as indicated. Below each condition is the term used for the memory state, given the indicated treatment conditions. *$p <$ 0.05, ****$p < 0.0001$ for all data as analyzed by one-way analysis of variance with Tukey's multiple comparisons test ($n = 29$, 40, 29, and 28, left to right, respectively, for panel B and $n =$ 59, 20, and 46, left to right, respectively, for panel C). (C) Immunohistochemistry images of OSCC, noting tumor core (TC) and invasive boarder zone (IZ), which was stained for phosphorylated AKT(s308); white dashed line indicates the boarder. Inset images are shown and correspond to their regions *i* and *ii* in the TC and IZ, respectively. White arrowheads indicate positive staining in the inset image. Scale bar is 100 μm. (D) Plot indicating the percentage of positively staining cells per field for OSCC tumors based on their tumor grade. Data are sorted by the presence of organized collagen from SHG imaging, as a surrogate for stiff matrix (orange), or absence (purple), as well as location within the tumor, that is, IZ (open data) and TC (filled data). Lines indicate average and SD. *$p < 0.05$ as analyzed by one-way analysis of variance with Tukey's multiple comparisons test. LPA, lysophosphatidic acid.

had more adhesion turnover and higher and more dynamic contractility, which make them more propulsive (Beri *et al.*, 2020) and able to sense and migrated against mechanical gradients (Yeoman *et al.*, 2021) relative to more strongly adherent cells. This process is also aided by supporting cells, for example, cancer-associated fibroblasts, which use traction forces generated by NMM2 to align and stiffen matrix to facilitate tumor invasion by the same mechanisms (Erdogan *et al.*, 2017). Although stiffness-based observations have occurred over the last decade, there is even more evidence from chemical modulation of contractility. LPA enhances ovarian (Sawada *et al.*, 2002) and prostate (Wang *et al.*, 2004) cell migration and invasion via Rho and ROCK in a manner that similarly regulates focal adhesion dynamics. We found that NMM2A expression increased after epithelial Cal27 cells were conditioned by LPA, which also made them more mesenchymal, migratory, and invasive, and conversely with Blebbistatin, blocking myosin activity prevented the mesenchymal phenotype. From these functional assays, we could conclude that cells can learn not only from the stiffness of matrix but also from contractility itself. More importantly for invasive, we further found that phenotype was maintained even in a new niche as "memory." Matrix rigidity may also feedback on itself to enhance cell contractility (Huang and Ingber, 2005), so it is conceivable that Cal27 cells could continuously gain mechanical memory so long as they are in the stiff matrix of the tumor core, suggesting that the cells that leave the tumor after increasing instruction could be even more virulent than their early disseminating counterparts. This concept, of course, would require significantly more complex in vivo labeling assays and tumor stiffness measurement to prove.

To understand how cells learn mechanical memory from the niche, we further examined which intracellular signaling pathways are involved. From the phospho-kinase array, we concluded that AKT and FAK signaling pathways are highly activated during memory learning and recovery phase, respectively. AKT activation has been observed in OSCC cells where the TRPV4 (Ca2+-permeable nonselective cation channel) expression level was high (Lee *et al.*, 2017; Sharma *et al.*, 2019; Fujii *et al.*, 2020). Since TRPV4 is mechanosensitive, the activation cascade from TRPV4 to AKT signaling pathway could have been possible during 5 d of conditioning in stiff matrix. Here, we found that AKT was necessary to acquire mechanical memory, since AKT inhibition decreased cell migration speed during preconditioning and in patients where phosphorylation was associated preferentially with tumor cores in the highest-grade tumors containing organized collagen. Conversely, we found that memory recovery in new niche depended on FAK phosphorylation. FAK has a critical function on adhesive complexes formation, cell shape, adhesion, and motility (Lauffenburger and Horwitz, 1996; Ridley *et al.*, 2003; Mitra *et al.*, 2005). Highly activated FAK can also up-regulate Rho GTPases, which enhances cytoskeleton organization (Mitra *et al.*, 2005; Mitra and Schlaepfer, 2006; Seong *et al.*, 2013). These features are all related to invasiveness of cells, and accordingly, mechanical memory remaining in the cell and recovered as a form of highly phosphorylated FAK allowed cells to keep invasive features.

Signals further downstream of kinases must ultimately result in transcriptional changes, which we found to correlate to patient outcomes, and are controlled by epigenetic marks in cells. As dysplastic regions evolve into invasive OSCC, cells acquire EMT markers, for example, vimentin (Webber *et al.*, 2017), concurrently with methylation at H3K4 (Rogenhofer *et al.*, 2013) and H3K27 (Chen *et al.*, 2013), but lose acetylation at H3K4 (Chen *et al.*, 2013) and H3K9ac. OSCC tumors in the lowest and highest quartiles of percent H3K9ac$^+$ cells showed markedly different disease outcomes (Webber *et al.*, 2017). These data suggest that an acetylation-to-methylation switch accompanies disease progression, and it may be concurrent with

the establishment of stiffness and memory. However, further assessment beyond the work here is needed to determine whether niche stiffness plays a role and which genes are affected. Although these data suggest that mechanical memory could involve histone modification, we believe that fundamentally our data here established a critical point; similar to other more well studied systems, for example, breast (Nasrollahi *et al.*, 2017), oral epithelial cells appear plastic, sensitive to stiffness, and after prolonged culture in stiffened niche, they retain a durable phenotype that is maintained in soft tumor–adjacent epithelial, which could facilitate invasion.

MATERIALS AND METHODS

Request a protocol through *Bio-protocol*.

Human biopsies

The experimental design and the informed consent procedures were approved by the Ethical Committee of Federal University of Rio Grande do Sul—Brazil and of Hospital de Clínicas de Porto Alegre (HCPA)—Brazil (GPPG n° 11-0289; GPPG n° 14-0019) and all patients in this study provided written informed consent. Patients ($n = 19$) with oral lesions were interviewed and submitted to surgery. OSCC diagnosis was confirmed histopathologically by a pathologist and fragments from regions corresponding to the center of the tumor, invasive zone, and the carcinoma edge tissue, that is, tumor-adjacent epithelia, were collected. Patient metadata are described in Supplemental Table S5.

Cell culture and reagents

OSCC cell lines were a kind gift from Akihiro Sakai, University of California San Diego (UCSD). Cal27 cells were cultivated in DMEM high glucose (Life Technologies) supplemented with 10% fetal bovine serum (FBS) (Gemini Bio) and 1% penicillin/streptomycin (Life Technologies); SCC25 cells were maintained in DMEM/F12 with 15-mM HEPES (Teknova) supplemented with 10% FBS, 1% penicillin/streptomycin, and 400 ng/ml hydrocortisone (Sigma). Cells were maintained in incubator at 37°C with 5% CO_2. The cells were selectively treated with Blebbistatin (up to 10 µM, Cayman Chemical), LPA (up to 10 µM, Enzo Life Sciences), Perifosine, AKT inhibitor (0.5 and 5 µM, InvivoGen), and FAK inhibitor 14 (1 and 10 µM, Sigma-Aldrich).

Mechanical and chemical cell conditioning on polyacrylamide hydrogels

Cal27 cells underwent 5 d of conditioning phase and a day of replating phase. After cells were seeded on collagen-coated polyacrylamide hydrogels (PA; 0.5 or 20 kPa), media was changed every day. PA hydrogels were fabricated and matrix proteins, for example, collagen type I, were attached using well-established protocols (Tse and Engler, 2010). Briefly, PA hydrogels were made on 12-mm or 25-mm glass coverslips that had been methacrylated by first oxidizing the surface through UV/ozone exposure (BioForce Nanosciences), followed by functionalization with 20-mM 3-(trimethoxysilyl) propyl methacrylate (Sigma-Aldrich, cat # 440159) in ethanol. A polymer solution containing either 3%/0.06% acrylamide/bis-acrylamide (Fisher) for 0.5 kPa hydrogels or 8%/0.264% for 20 kPa hydrogels, 1% vol/vol of 10% ammonium persulfate (Fisher), and 0.1% vol/vol of N,N,N′,N′-tetramethylethylenediamine (VWR) was prepared. Approximately 15 µl for 12-mm coverslips and 30 µl for 25-mm coverslips of hydrogel solution were sandwiched between a functionalized coverslip and a dichlorodimethylsilane-treated glass slide and polymerized for 10 and 30 min, respectively, for 20 kPa and 0.5 kPa gels. Hydrogels were incubated in 0.2 mg/ml sulfo-SANPAH (Fisher, cat #22589) in sterile 50-mM HEPES pH 8.5, activated with UV light (wavelength 350 nm, intensity 4 mW/cm^2) for 10 min, washed three times in PBS, and then incubated in 150 µg/ml collagen solution (Corning) overnight at 37°C.

LPA, Blebbistatin, or Perifosin was also selectively applied during the conditioning phase. After 5 d of conditioning, cells were trypsinized with 0.25% trypsin-EDTA for 20 min at 37°C, 5% CO_2, and replated on soft (0.5 kPa) gels to be incubated one more day at 37°C, 5% CO_2. FAK inhibitor 14 was applied during replating phase.

Real-time PCR

RNA was extracted from cells using using RNeasy Mini Kit (Qiagen) and total RNA quantity and quality were checked via A280/A260 ratio. Reverse transcription was performed with SuperScript IV Reverse Transcriptase (ThermoFisher Scientific, #180090010) on 2 µg of RNA template. Quantitative PCR was performed (45 cycles, 95°C for 15 s, followed by 60°C for 1 min) using a 7900HT Fast Real-Time PCR System (Thermo) with the primer sets described in Supplemental Table S6 and PowerSYBR Green Supermix (Applied Biosystems, #436759). Target genes expressed in experimental groups were normalized with genes (including *GAPDH* as housekeeping gene) expressed in native Cal27 as control using delta-delta-Ct method.

Migration assay

OSCC cells were plated on either 0.5 or 20 kPa PA hydrogels for 12 h and were then imaged with a Nikon Eclipse Ti-S microscope equipped with a motorized temperature- and CO_2-controlled stage. Cells were imaged at 10× in brightfield at multiple positions every 15 min for 24 h. For analysis of migration parameters, the nucleus of each migratory cell was used as a reference point to track each cell with the "Manual Tracking" plugin on ImageJ. Migration was considered to be in single-cell mode when a cell did not touch any other cell during its migration movement. Migration was considered to be in collective-cell mode when cells migrated in a group of two or more cells.

Phospho-kinase array

Protein phosphorylation was examined using a membrane-based sandwich immunoassay (Proteome Profiler Array, R&D Systems, #ARY003C) according to the manufacturers' instructions. Briefly, total Cal27 cells were trypsinized after 5 d in soft (0.5 kPa) or stiff (20 kPa) substrate and replated in another stiffness for 1 h in six-well plates. Cells plated in the same substrate after 5 d were used as a control. Lysates were made from cultures and a total of 300-µg protein was then incubated with the Human Phospho-Kinase Array. The proteins present in a lysate sample were captured by discrete antibodies printed in duplicate across the nitrocellulose membranes. The array was washed 3× with buffer for 10 min on a rocking platform shaker and then incubated with a cocktail of biotinylated detection antibodies and subsequent application of streptavidin-HRP conjugate. The signals were detected with Chemi Reagent Mix (R&D Systems, Abingdon, Oxford, UK). Developed signals were analyzed using ImageJ analysis software.

Western blotting

Cells were lysed with mRIPA buffer and total amount of protein was measured by BCA assay kit (Pierce; #23225). Approximately 10–15 µg of protein per sample was denatured by 4× Laemlli sample buffer and heated at 95°C for 5 min. Samples were loaded to only 5% Bis-Tris gels and underwent electrophoresis under 140 V for 1.5 h. Proteins on gel were blotted to nitrocellulose membrane using iBlot semidry transfer system (Invitrogen, #IB21000). The membrane

was blocked for an hour at room temperature. The membrane was first immunoassayed with primary antibody at 4°C for 24 h to detect NMM2A (1:500, Cell Signaling, #3403), NMM2B (1:500, Cell Signaling, #8824), NMM2C (1:500, Cell Signaling, #8189), E-cadherin (1:1000, Cell Signaling, #3915), N-cadherin (1:1000, Cell Signaling, #13116), pFAK (1:1000, Cell Signaling, #3283), MLCK (1:1000, Sigma-Aldrich, #SAB4200808), and Tubulin (Sigma-Aldrich, #SAB4500088). After overnight incubation, the membrane was rinsed with buffer three times, 5 min per rinse. The membrane was incubated with Alexa Fluor 680 donkey antimouse (1:5000, Invitrogen, A10038) and Alexa Fluor 790 donkey antirabbit (1:5000, Invitrogen, A11374) diluted by blocking buffer for an hour at room temperature. Image was acquired by LI-COR Odyssey CLx imaging software and analyzed by Image Studio Lite.

Immunofluorescence

After conditioning and replating phase, Cal27 were fixed on the PAAGS (3.7% paraformaldehyde, 15 min, RT). In addition to conditioned cells, Cal27 and SCC25 were fixed after overnight incubation on gel to be used as control. Cells were washed with PBS (3×, 10 min each), permeabilized (30 min) with 0.5% Triton X in Solution A, and blocked (30 min) with 0.1% Triton X in buffer (0.3-M Glycine, 10% FBS, and 1% Bovine Serum Albumin in Solution A). After rinsing (3×, 10 min each) with Solution A, anti-E-Cadherin (1:200, Cell Signaling, #3915) and anti-NMM2A (1:50, Cell Signaling, #3403) antibodies in IF buffer were applied to fixed samples and incubated overnight at 4°C. After rinsing with Solution A (3×, 10 min each), samples were selectively stained with antirabbit (1:500, 1:500, ThermoFisher Scientific, #A-11008) or antimouse (1:500, ThermoFisher Scientific, #A28175) secondary antibodies for 2 h at room temperature. Nuclei and actin staining was done with DAPI (1:1000, Tocris, #5748) and rhodamine–phalloidin (1:250, Cytoskeleton., #PHDR1) for 20 min at room temperature on shaker. After staining, samples were rinsed once with 0.5% Triton X in solution A (5 min), twice with solution A (10 min each), and once with DI water. Samples prepared on coverslip were mounted on microscope slide with fluoromount, and images were acquired by Keyence BZ-X800 microscope.

ImageJ was used to analyze immunofluorescent images. For E-cadherin–stained samples, images had their background subtracted. Then, the edge of each cell was traced in the actin channel and pixel intensity with respect to the radial distance from the center of the cell was measured in E-cadherin channel with "Radial Profile" plugin in ImageJ. Cells with aspect ratio below 2 were used for analysis to remove the measurement error due to cell morphology. For each cell, pixel intensity for pixels within the first and last 5% of the cell radius was averaged and plotted as a ratio of edge/center. For NMM2-stained samples, average intensity per cell was plotted and normalized to the batch average for control SCC25 cells.

RNA sequencing

RNA from Cal27 cells cultured in "Learn" versus "Don't Learn" or "Forget" conditions was collected by RNeasy Minit Kit (QIAGEN, 74104). The purified RNA was then processed by the Institute for Genomic Medicine at University California San Diego. RNA integrity was analyzed using an Agilent Tape station system and precise RNA concentration determined using a Qubit 2.0 Fluorometer. Libraries were built using the Illumina TruSeq Stranded RNA, High Throughput Library Prep Kit and sequenced on a NovaSeq 6000 for samples with RIN numbers at 9.0 and above. RNA-sequencing data were analyzed by ROSALIND (https://rosalind.onramp.bio/), with a HyperScale architecture (ROSALIND, San Diego, CA). Reads were trimmed using cutadapt (Martin, 2011). Quality scores were assessed using FastQC (Babraham Bioinformatics, Cambridge, UK). Reads were aligned to the human genome build dm6 using STAR (Dobin *et al.*, 2013). Individual sample reads were quantified using HTseq (Anders *et al.*, 2015) and normalized via Relative Log Expression using DESeq2 R library (Love *et al.*, 2014). DEseq2 was also used to calculate fold changes and *p* values and perform optional covariate correction. Clustering of genes for the final heat map of DEGs was done using the Partitioning Around Medoids method using the fpc R library. Functional enrichment analysis of pathways, gene ontology, domain structure, and other ontologies were performed using HOMER (Duttke *et al.*, 2019). Enrichment was calculated relative to a set of background genes relevant for the experiment. Panther was used to assess GO terms for gene lists generated in ROSALIND.

TCGA data set analysis

TCGA raw data were directly downloaded from NIH NCI GDC Data portal. Corresponding clinical metadata were obtained from a previous publication (Liu *et al.*, 2018). Among the patient data with head-neck squamous carcinoma, those whose primary site is either base of tongue or other and unspecified parts of tongue were used for analysis. The 5-y survival rate of patients was correlated with gene expression corresponding to "Learn" or "Don't Learn/Forget." Expression of the differentially expressed gene between "Learn" and "Don't Learn/Forget" subgroups was normalized by z-score based on the mean of each gene expression across the whole patient data. For every patient, z-score of all DEG was summed, and z-score–based quintiles were mapped to "Learn" and "Don't Learn/Forget" categories. The Kaplan–Meier method was used to create overall survival and progression-free interval comparing the top and bottom quantile of patient data. To determine the significance of survival rate difference between two groups, log-rank test was used. Survival analysis includes the Lifelines python library (https://lifelines.readthedocs.io/en/latest/).

Data availability

Data generated in this study were deposited to NCBI under GEO207685. We do not impose any restrictions on data availability. Relevant scripts for the analysis of TCGA data are available at: https://github.com/englea52/OSCC_Memory.git

Statistics

All data are shown from triplicate biological replicates with the total number of measurements made indicated in figure legends. For *qPCR* gene expression, 2D migration assays, 3D spheroid invasion, and immunofluorescence and immunohistological quantification, data were analyzed by one-way analysis of variance with Tukey's posttest or multiple comparisons test as indicated. For all analyses, $*p < 0.05$, $**p < 0.01$, $***p < 0.001$, and $****p < 0.0001$. Significance for TCGA analyses was performed with a log-rank (Mantel–Cox) test. Data expressed as box-and-whisker plots show all points with the mean and whisker ends corresponding to minimum and maximum values. All other values are expressed as mean ± SD. Statistical analyses were performed using Prism software.

ACKNOWLEDGMENTS

The authors thank Dr. Kristen Jepsen of the Institute for Genomic Medicine (UC San Diego) for assistance with sequencing, Drs. Meghana Pagadala and Hannah Carter (UC San Diego) for assistance with TCGA analyses, and Maya Levitan (Rice University) for experimental assistance. The results shown here are in part based upon data generated by the TCGA Research Network: https://www.cancer.gov/tcga. The authors acknowledge funding support from

the U.S. National Institutes of Health (R01CA206880 to A.J.E.), the U.S. National Science Foundation (CMMI-1763139 to A.J.E.), and the American Cancer Society Institutional Research Grant (15-172-45-IRG) provided through the Moores Cancer Center at the University of California San Diego. This publication includes data generated at the UC San Diego IGM Genomics Center utilizing an Illumina NovaSeq 6000 that was purchased with funding from a National Institutes of Health SIG grant (S10OD026929). Student support was provided by the Kwanjeong Educational Foundation (to S.Y.M.) and the Coordenação de Aperfeiçoamento de Pessoal de Nível Superior—Brazil (CAPES)—Finance Code 001 (to P.S.C.). Funding agencies were not involved in experimental design.

REFERENCES

Aguilar-Cuenca R, Juanes-García A, Vicente-Manzanares M (2014). Myosin II in mechanotransduction: master and commander of cell migration, morphogenesis, and cancer. Cell Mol Life Sci 71, 479–492.

Alonso-Nocelo M, Raimondo TM, Vining KH, López-López R, De La Fuente M, Mooney DJ (2018). Matrix stiffness and tumor-associated macrophages modulate epithelial to mesenchymal transition of human adenocarcinoma cells. Biofabrication 10, 035004.

Anders S, Pyl PT, Huber W (2015). HTSeq—a Python framework to work with high-throughput sequencing data. Bioinformatics 31, 166–169.

Baker AM, Bird D, Lang G, Cox TR, Erler JT (2013). Lysyl oxidase enzymatic function increases stiffness to drive colorectal cancer progression through FAK. Oncogene 32, 1863–1868.

Beri P, Popravko A, Yeoman B, Kumar A, Chen K, Hodzic E, Chiang A, Abnisadr A, Placone JK, Carter H, *et al.* (2020). Cell adhesiveness serves as a biophysical marker for metastatic potential. Cancer Res 80, 901–911.

Bonnans C, Chou J, Werb Z (2014). Remodelling the extracellular matrix in development and disease. Nat Rev Mol Cell Biol 15, 786–801.

Boudreau A, Van't Veer LJ, Bissell MJ (2012). An "elite hacker": breast tumors exploit the normal microenvironment program to instruct their progression and biological diversity. Cell Adh Migr 6, 236–435.

Bray F, Ferlay J, Soerjomataram I, Siegel RL, Torre LA, Jemal A (2018). Global cancer statistics 2018: GLOBOCAN estimates of incidence and mortality worldwide for 36 cancers in 185 countries. CA Cancer J Clin 68, 394–424.

Burgstaller G, Oehrle B, Gerckens M, White ES, Schiller HB, Eickelberg O (2017). The instructive extracellular matrix of the lung: basic composition and alterations in chronic lung disease. Eur Respir J 50, 1601805.

Butcher DT, Alliston T, Weaver VM (2009). A tense situation: forcing tumour progression. Nat Rev Cancer 9, 108–122.

Calvo F, Ege N, Grande-Garcia A, Hooper S, Jenkins RP, Chaudhry SI, Harrington K, Williamson P, Moeendarbary E, Charras G, Sahai E (2013). Mechanotransduction and YAP-dependent matrix remodelling is required for the generation and maintenance of cancer-associated fibroblasts. Nat Cell Biol 15, 637–646.

Chaudhuri O, Koshy ST, Branco Da Cunha C, Shin JW, Verbeke CS, Allison KH, Mooney DJ (2014). Extracellular matrix stiffness and composition jointly regulate the induction of malignant phenotypes in mammary epithelium. Nat Mater 13, 970–978.

Chen Y, Terajima M, Yang Y, Sun L, Ahn YH, Pankova D, Puperi DS, Watanabe T, Kim MP, Blackmon SH, *et al.* (2015). Lysyl hydroxylase 2 induces a collagen cross-link switch in tumor stroma. J Clin Invest 125, 1147–1162.

Chen YW, Kao SY, Wang HJ, Yang MH (2013). Histone modification patterns correlate with patient outcome in oral squamous cell carcinoma. Cancer 119, 4259–4267.

Chi AC, Day TA, Neville BW (2015). Oral cavity and oropharyngeal squamous cell carcinoma—an update. CA Cancer J Clin 65, 401–421.

Chin LK, Xia Y, Discher DE, Janmey PA (2016). Mechanotransduction in cancer. Curr Opin Chem Eng 11, 77–84.

Dias KB, Flores APC, Hildebrand LDC, De Oliveira MG, Lamers ML, Rados PV, Magnusson AS, Filho MS (2019). Non-muscle myosin II as a predictive factor in head and neck squamous cell carcinoma. Med Oral Patol Oral Cir Bucal 24, e346–e353.

Dobin A, Davis CA, Schlesinger F, Drenkow J, Zaleski C, Jha S, Batut P, Chaisson M, Gingeras TR (2013). STAR: ultrafast universal RNA-seq aligner. Bioinformatics 29, 15–21.

Duttke SH, Chang MW, Heinz S, Benner C (2019). Identification and dynamic quantification of regulatory elements using total RNA. Genome Res 29, 1836–1846.

Erdogan B, Ao M, White LM, Means AL, Brewer BM, Yang L, Washington MK, Shi C, Franco OE, Weaver AM, *et al.* (2017). Cancer-associated fibroblasts promote directional cancer cell migration by aligning fibronectin. J Cell Biol 216, 3799–3816.

Fattet L, Jung HY, Matsumoto MW, Aubol BE, Kumar A, Adams JA, Chen AC, Sah RL, Engler AJ, Pasquale EB, Yang J (2020). Matrix rigidity controls epithelial-mesenchymal plasticity and tumor metastasis via a mechanoresponsive EPHA2/LYN complex. Dev Cell 54, 302–316.e7.

Frantz C, Stewart KM, Weaver VM (2010). The extracellular matrix at a glance. J Cell Sci 123, 4195–4200.

Friedl P, Locker J, Sahai E, Segall JE (2012). Classifying collective cancer cell invasion. Nat Cell Biol 14, 777–783.

Fujii S, Tajiri Y, Hasegawa K, Matsumoto S, Yoshimoto RU, Wada H, Kishida S, Kido MA, Yoshikawa H, Ozeki S, Kiyoshima T (2020). The TRPV4-AKT axis promotes oral squamous cell carcinoma cell proliferation via CaMKII activation. Lab Investig 100, 311–323.

Geiger B, Bershadsky A, Pankov R, Yamada KM (2001). Transmembrane crosstalk between the extracellular matrix–cytoskeleton crosstalk. Nat Rev Mol Cell Biol 2, 793–805.

Hanahan D, Weinberg RA (2011). Hallmarks of cancer: the next generation. Cell 144, 646–674.

Huang S, Ingber DE (2005). Cell tension, matrix mechanics, and cancer development. Cancer Cell 8, 175–176.

Jensen JS, Jakobsen KK, Mirian C, Christensen JT, Schneider K, Nahavandipour A, Wingstrand BL, Wessel I, Tvedskov JF, Frisch T, *et al.* (2019). The Copenhagen Oral Cavity Squamous Cell Carcinoma database: protocol and report on establishing a comprehensive oral cavity cancer database. Clin Epidemiol 11, 733–741.

Johnson NW, Jayasekara P, Amarasinghe AA, Hemantha K (2011). Squamous cell carcinoma and precursor lesions of the oral cavity: epidemiology and aetiology. Periodontol 2000 57, 19–37.

Kamangar F, Dores GM, Anderson WF (2006). Patterns of cancer incidence, mortality, and prevalence across five continents: defining priorities to reduce cancer disparities in different geographic regions of the world. J Clin Oncol 24, 2137–2150.

Lauffenburger DA, Horwitz AF (1996). Cell migration: a physically integrated molecular process. Cell 84, 359–369.

Lee WH, Choong LY, Jin TH, Mon NN, Chong S, Liew CS, Putti T, Lu SY, Harteneck C, Lim YP (2017). TRPV4 plays a role in breast cancer cell migration via Ca 2+-dependent activation of AKT and downregulation of E-cadherin cell cortex protein. Oncogenesis 6, e338–e338.

Levental KR, Yu H, Kass L, Lakins JN, Egeblad M, Erler JT, Fong SFT, Csiszar K, Giaccia A, Weninger W, *et al.* (2009). Matrix crosslinking forces tumor progression by enhancing integrin signaling. Cell 139, 891–906.

Liu J, Lichtenberg T, Hoadley KA, Poisson LM, Lazar AJ, Chemiack AD, Kovatich AJ, Benz CC, Levine BA, Lee AV, *et al.* (2018). An integrated TCGA pan-cancer clinical data resource to drive high-quality survival outcome analytics. Cell 173, 400–416.e11.

Love MI, Huber W, Anders S (2014). Moderated estimation of fold change and dispersion for RNA-seq data with DESeq2. Genome Biol 15, 550.

Lu P, Weaver VM, Werb Z (2012). The extracellular matrix: a dynamic niche in cancer progression. J Cell Biol 196, 395.

Martin M (2011). Cutadapt removes adapter sequences from high-throughput sequencing reads. EMBnet J 17, 10–12.

Matte BF, Kumar A, Placone JK, Zanella VG, Martins MD, Engler AJ, Lamers ML (2019). Matrix stiffness mechanically conditions EMT and migratory behavior of oral squamous cell carcinoma. J Cell Sci 132, jcs224360.

Mitra SK, Hanson DA, Schlaepfer DD (2005). Focal adhesion kinase: in command and control of cell motility. Nat Rev Mol Cell Biol 6, 56–68.

Mitra SK, Schlaepfer DD (2006). Integrin-regulated FAK-Src signaling in normal and cancer cells. Curr Opin Cell Biol 18, 516–523.

Montero PH, Patel SG (2015). Cancer of the oral cavity. Surg Oncol Clin N Am 24, 491–508.

Nasrollahi S, Walter C, Loza AJ, Schimizzi GV, Longmore GD, Pathak A (2017). Past matrix stiffness primes epithelial cells and regulates their future collective migration through a mechanical memory. Biomaterials 146, 146–155.

Newell-Litwa KA, Horwitz R, Lamers ML (2015). Non-muscle myosin II in disease: mechanisms and therapeutic opportunities. Dis Model Mech 8, 1495–1515.

Ondeck MG, Kumar A, Placone JK, Plunkett CM, Matte BF, Wong KC, Fattet L, Yang J, Engler AJ (2019). Dynamically stiffened matrix promotes malignant transformation of mammary epithelial cells via collective mechanical signaling. Proc Natl Acad Sci USA 116, 3502–3507.

Parsons JT, Horwitz AR, Schwartz MA (2010). Cell adhesion: integrating cytoskeletal dynamics and cellular tension. Nat Rev Mol Cell Biol 11, 633–643.

Paszek MJ, Zahir N, Johnson KR, Lakins JN, Rozenberg) GI, Gefen A, Reinhart-King CA, Margulies SS, Dembo M, Boettiger D, *et al.* (2005). Tensional homeostasis and the malignant phenotype. Cancer Cell 8, 241–254.
Peglion F, Llense F, Etienne-Manneville S (2014). Adherens junction treadmilling during collective migration. Nat Cell Biol 16, 639–651.
Pickup MW, Mouw JK, Weaver VM (2014). The extracellular matrix modulates the hallmarks of cancer. EMBO Rep 15, 1243–1253.
Pires FR, Ramos AB, de Oliveira JBC, Tavares AS, de Luz PSR, dos Santos TCRB (2013). Oral squamous cell carcinoma: clinicopathological features from 346 cases from a single oral pathology service during an 8-year period. J Appl Oral Sci 21, 460–467.
Ridley AJ, Schwartz MA, Burridge K, Firtel RA, Ginsberg MH, Borisy G, Parsons JT, Horwitz AR (2003). Cell migration: integrating signals from front to back. Science 302, 1704–1709.
Rogenhofer S, Miersch H, Göke F, Kahl P, Wieland WF, Hofstädter F, Kristiansen G, Von Ruecker A, Müller SC, Ellinger J (2013). Histone methylation defines an epigenetic entity in penile squamous cell carcinoma. J Urol 189, 1117–1122.
Sawada K, Morishige K, Tahara M, Ikebuchi Y, Kawagishi R, Tasaka K, Murata Y (2002). Lysophosphatidic acid induces focal adhesion assembly through Rho/Rho-associated kinase pathway in human ovarian cancer cells. Gynecol Oncol 87, 252–259.
Scully C, Bagan J (2009). Oral squamous cell carcinoma overview. Oral Oncol 45, 301–308.
Seong J, Wang N, Wang Y (2013). Mechanotransduction at focal adhesions: from physiology to cancer development. J Cell Mol Med 17, 597–604.
Sharma S, Goswami R, Zhang DX, Rahaman SO (2019). TRPV4 regulates matrix stiffness and TGFβ1-induced epithelial-mesenchymal transition. J Cell Mol Med 23, 761–774.
Stowers RS, Shcherbina A, Israeli J, Gruber JJ, Chang J, Nam S, Rabiee A, Teruel MN, Snyder MP, Kundaje A, Chaudhuri O (2019). Matrix stiffness induces a tumorigenic phenotype in mammary epithelium through changes in chromatin accessibility. Nat Biomed Eng 3, 1009–1019.
Tilghman RW, Cowan CR, Mih JD, Koryakina Y, Gioeli D, Slack-Davis JK, Blackman BR, Tschumperlin DJ, Parsons JT (2010). Matrix rigidity regulates cancer cell growth and cellular phenotype. PLoS One 5, e12905.
Tse JR, Engler AJ (2010). Preparation of hydrogel substrates with tunable mechanical properties. Curr Protoc Cell Biol Chapter 10, Unit 10.16.
Umesh V, Rape AD, Ulrich TA, Kumar S (2014). Microenvironmental stiffness enhances glioma cell proliferation by stimulating epidermal growth factor receptor signaling. PLoS One 9, e101771.
Van Helvert S, Storm C, Friedl P (2018). Mechanoreciprocity in cell migration. Nat Cell Biol 20, 8–20.
Vicente-Manzanares M, Koach MA, Whitmore L, Lamers ML, Horwitz AF (2008). Segregation and activation of myosin IIB creates a rear in migrating cells. J Cell Biol 183, 543–554.
Wang N, Tytell JD, Ingber DE (2009). Mechanotransduction at a distance: mechanically coupling the extracellular matrix with the nucleus. Nat Rev Mol Cell Biol 10, 75–82.
Wang Q, Liu M, Kozasa T, Rothstein JD, Sternweis PC, Neubig RR (2004). Thrombin and lysophosphatidic acid receptors utilize distinct rhoGEFs in prostate cancer cells. J Biol Chem 279, 28831–28834.
Warnakulasuriya S (2009). Global epidemiology of oral and oropharyngeal cancer. Oral Oncol 45, 309–316.
Webber LP, Wagner VP, Curra M, Vargas PA, Meurer L, Carrard VC, Squarize CH, Castilho RM, Martins MD (2017). Hypoacetylation of acetyl-histone H3 (H3K9ac) as marker of poor prognosis in oral cancer. Histopathology 71, 278–286.
Wei SC, Fattet L, Tsai JH, Guo Y, Pai VH, Majeski HE, Chen AC, Sah RL, Taylor SS, Engler AJ, Yang J (2015). Matrix stiffness drives epithelial-mesenchymal transition and tumour metastasis through a TWIST1-G3BP2 mechanotransduction pathway. Nat Cell Biol 17, 678–688.
Wei X, Lou H, Zhou D, Jia Y, Li H, Huang Q, Ma J, Yang Z, Sun C, Meng Y, *et al.* (2021). TAGLN mediated stiffness-regulated ovarian cancer progression via RhoA/ROCK pathway. J Exp Clin Cancer Res 40, 292.
Wong SY, Ulrich TA, Deleyrolle LP, MacKay JL, Lin JMG, Martuscello RT, Jundi MA, Reynolds BA, Kumar S (2015). Constitutive activation of myosin-dependent contractility sensitizes glioma tumor-initiating cells to mechanical inputs and reduces tissue invasion. Cancer Res 75, 1113–1122.
Wozniak MA, Chen CS (2009). Mechanotransduction in development: a growing role for contractility. Nat Rev Mol Cell Biol 10, 34–43.
Wu YI, Frey D, Lungu OI, Jaehrig A, Schlichting I, Kuhlman B, Hahn KM (2009). A genetically encoded photoactivatable Rac controls the motility of living cells. Nature 461, 104–108.
Yamada KM, Sixt M (2019). Mechanisms of 3D cell migration. Nat Rev Mol Cell Biol 20, 738–752.
Yeoman B, Shatkin G, Beri P, Banisadr A, Katira P, Engler AJ (2021). Adhesion strength and contractility enable metastatic cells to become adurotactic. Cell Rep 34, 108816.
Yu M, Shen W, Shi X, Wang Q, Zhu L, Xu X, Yu J, Liu L (2019). Upregulated LOX and increased collagen content associated with aggressive clinicopathological features and unfavorable outcome in oral squamous cell carcinoma. J Cell Biochem 120, 14348–14359.
Zhang B, Gao S, Li R, Li Y, Cao R, Cheng J, Guo Y, Wang E, Huang Y, Zhang K (2020). Tissue mechanics and expression of TROP2 in oral squamous cell carcinoma with varying differentiation. BMC Cancer 20, 815.
Zhang JY, Zhu WW, Wang MY, Zhai RD, Wang Q, Shen WL, Liu LK (2021). Cancer-associated fibroblasts promote oral squamous cell carcinoma progression through LOX-mediated matrix stiffness. J Transl Med 19, 513.